Flow regimes in T-shaped micro-mixers.

Tommaso Andreussi[a], Chiara Galletti[b,*], Roberto Mauri[b], Simone Camarri[b], Maria Vittoria Salvetti[b]

[a] *ALTA S.p.A., Pisa, Italy.*
[b] *Department of Civil and Industrial Engineering, University of Pisa, Italy.*

Abstract

The different flow regimes occurring in T-mixers are investigated by means of direct numerical simulations. Three different values of the aspect ratio of the inlet channels, κ_i, that is their width to height ratio are considered, namely $\kappa_i = 0.75, 1$ and 2. For the configurations with $\kappa_i = 0.75$ and 1, the same behavior as previously described in the literature, is found. In particular, as the Reynolds number is increased, the flow evolves from vortical to engulfment steady regimes, then to unsteady asymmetric and symmetric periodic regimes, until, finally, it becomes chaotic. All the critical values of the Reynolds number, at which the transitions between the different regimes occur, are found to be very similar for $\kappa_i = 0.75$ and 1, while some differences are highlighted in the vorticity dynamics and characteristic frequencies of the unsteady regimes. The observed scenario is completely different for $\kappa_i = 2$. Indeed, in this case, the flow evolves directly from the vortical regime to an unsteady symmetric behavior, with a vorticity dynamics that is significantly different from those observed for the other aspect ratios.

Keywords: micro-reactors, engulfment, flow instabilities, laminar flow.

*corresponding author, email: chiara.galletti@unipi.it

PACS:

1. Introduction

Fast and efficient mixing at the microscale is important in many unit operations encountered in the process industry as well as in the biological field. Applications range from miniature fuel cells to molecular diagnostics and, in general, to any micro-reactors, where a fast homogenization of reactants is required. As these microfluidic devices should be inexpensive and simple to operate, such features are fulfilled by passive micro-mixers, where mixing is promoted by without the help of any external power source (Kumar et. al., 2011). One of the simplest designs of passive micro-mixers is a T shape, in which the inlets join the main channel with T-shaped branches. This type of mixer is also suitable for carrying out fundamental studies, as the T-shaped micro-mixer is often encountered as a junction element in more complex micro-systems. The characteristics of these devices and, in particular, their efficiency in effectively mixing two liquid streams, has been largely studied in previous investigations. So far, different flow regimes have been identified, depending on the Reynolds number, Re, namely: the stratified, the vortex, the engulfment and the unsteady flow regimes (Engler et al., 2004; Hoffmann et al., 2006; Bothe et al., 2006, 2008; Dreher et al., 2009; Ooms et al., 2009; Thomas et al., 2010; Thomas and Ameel, 2010; Kockmann and Roberge, 2011; see also the review in Lindken et al., 2009). In the stratified flow regime, the inlet streams come in contact with one another in the mixing zone and then flow side by side through the mixing channel, resulting in a completely segregated fluid flow. In the vortex regime, above a critical Re, a secondary flow in the form of a double vortex pair occurs, due to the instabilities induced by the centrifugal forces at the confluence, leaving however the

two incoming streams well segregated. As Re is increased, the flow field goes through a bifurcation which drives the system from a perfectly symmetric flow to an asymmetric configuration, generally referred to as the engulfment regime. Here, the fluid elements at the confluence of the two inlet flows reach the opposite side of the mixing channel, thus largely increasing the degree of mixing. Many studies in the literature focused on the engulfment regime, because of the significant mixing efficiency achieved in this regime (see, e.g., Lindken et al., 2006, Soleymani et al., 2008; Ooms et al., 2009; Galletti et al., 2012; Fani et al., 2013; Poole et al., 2013). Finally, a few investigations have indicated that by further increasing Re, the flow becomes first unsteady and periodic in time and eventually chaotic (Dreher et al., 2009; Thomas et al., 2010; Thomas and Ameel, 2010; Kockmann and Roberge, 2011, Fani et al., 2014).

A fundamental parameter, together with the Reynolds number, that determines the appearance of different flow regimes is the geometry of the T-mixer, namely its aspect ratio. In T-mixers, two different aspect ratios can be defined: the inlet and the mixing channel aspect ratios ($\kappa_i = W_i/H$ and $\kappa_o = W_o/H$, respectively), where H is the channel depth, while W_i and W_o are the widths of the inlet and mixing channels, respectively. In most of the applications, $W_o = 2W_i$, so that $\kappa_o = 2\,\kappa_i$, in order to ensure the same bulk velocity in the inlet branches as in the outlet (mixing) channel.

The most investigated T-mixer configuration in the literature is the one with square inlets (i.e. $\kappa_i = 1$) and with $\kappa_o = 2\,\kappa_i$. Based on numerical simulations, Bothe et al. (2008) reported that when $Re > 240$ the flow exhibits a periodic behavior. Using this same geometric setup, Dreher et al.

(2009) confirmed that when $Re > 240$ the flow field becomes time periodic. In particular, they found that, when $240 < Re < 400$, this pulsating flow is characterized by a Strouhal number within the range $0.15 < St < 0.29$. Such periodic pulsations were found to disappear for larger Re, i.e. when $Re > 500$, where a chaotic, pseudo-turbulent motion was observed. Importantly, such instabilities were found to enhance the mixing process: indeed, optimum mixing was achieved for $240 < Re < 700$. The above findings were confirmed by Minakov et al. (2012, 2013) who numerically investigated a T-mixer with $\kappa_i = 1$ and observed a periodic behavior for $240 < Re < 400$, with Strouhal numbers $0.20 < St < 0.24$. When $400 < Re < 1000$, these authors observed a chaotic motion; however, upon increasing the length of the mixing channel, the oscillations were found to gradually fade away towards a laminar flow regime.

Experimentally, a clear evidence on the occurrence of unsteady motions was provided by Thomas et al. (2010) and Thomas and Ameel (2010), who investigated through planar and discrete-point Laser Induced Fluorescence the water-water mixing in a T-mixer with square inlets ($\kappa_i = 1$, $\kappa_o = 2\kappa_i$) for $56 < Re < 422$. When $Re > 195$, these authors observed an unsteady periodic behavior, characterized by an asymmetric co-rotating two-vortex topology. By further increasing the flow rate, i.e. when $Re > 350$, the flow switched to a symmetrical four-vortex topology, which had a detrimental effect on mixing.

Unsteady asymmetric and symmetric regimes, having features very similar to those found in the above mentioned experiments, were also detected in the simulations of Fani et al. (2014) for a T-mixer having an inlet aspect

ratio $\kappa_i = 0.75$.

Some efforts in the past have been made to derive correlations to predict the Reynolds number characterizing the onset of the steady asymmetric flow (engulfment regime) as a function of these two aspect ratios (Soleymani et al., 2008; Cherlo and Pushpavanam, 2010) although such correlations appear to be suited only for specific ranges of conditions (Galletti et al., 2012, Poole et al., 2013). Nonetheless, there is no systematic study in the literature on the effects of the inlet aspect ratio on the unsteady regimes. The present work is aimed at investigating the effect of the T-mixer geometry (i.e. the aspect ratios) on the flow regimes occurring in T-shaped micro-mixers, with particular attention devoted to the unsteady state regimes. To this aim, Direct Numerical Simulations were carried out by means of a high-order spectral element code which allows a massive parallelization, for $\kappa_i = 0.75$, 1 and 2. In particular, this last geometry is significantly different from the others and it has been only marginally investigated in the literature (Hoffmann et al., 2006).

2. Problem description and methodology

2.1. T-mixer geometry

The geometry of a T-mixer is illustrated in Figure 1 (not in scale), along with the coordinate axes. It consists of two inlet and one outlet channels, all with rectangular cross sections.

Three types of micro-mixer geometries were investigated, with the aspect ratio of the inlet channels, $\kappa_i = W_i/H$, equal to 0.75, 1 and 2. In all cases, the aspect ratio of the mixing channel, $\kappa_o = W_o/D$, is twice that of the

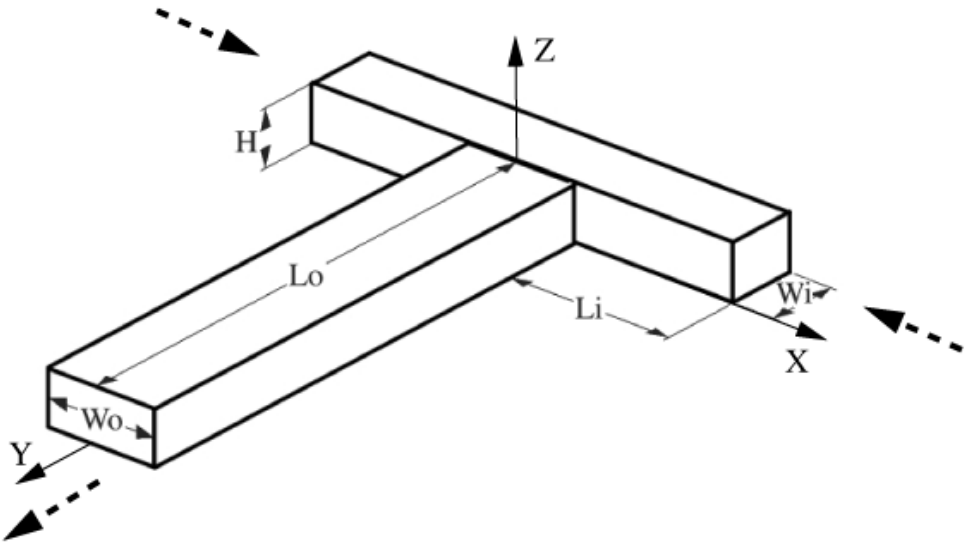

Figure 1: Sketch of the T-mixer

inlet channels, i.e. $\kappa_o = 2\kappa_i$, so that the mean velocity is the same in the inlet branches as in the outlet, mixing, conduit. A summary of all geometric characteristics is reported in Table 1, where the T-mixer dimensions are normalized using the hydraulic diameter of the mixing channel, D. In particular, the length of the inlet channels, L_i, was chosen to include the whole confluence region, while the length of the mixing channel, L_o, is long enough to ensure that the flow field is fully developed and the complex vortical structures are completely described. For the case with square inlet cross-sections (i.e., with $\kappa_i = 1$), the length of the mixing channel, L_o, was varied between $12.5D$ and $45D$, in order to assess the effect of this geometrical parameters on the onset of the different flow regimes. Note that $L_o = 12.5D$ was used in previous investigations (Galletti et al., 2012; Fani et al., 2013), while

Table 1: List of investigated T-mixer geometries

κ_i [-]	H/D [-]	W_o/D [-]	W_i/D[-]	L_i/D[-]	L_o/D [-]
0.75	0.625	2.5	1.25	2.25	25
1	0.75	1.5	0.75	2.25	12.5-45
2	0.833	1.25	0.625	6.25	25

$L_o = 25D$ was used in a recent work (Fani et al., 2014). Following the results of this sensitivity analysis, $L_o = 25D$ was adopted for the other two considered T-mixer configurations, i.e. for $k_i = 0.75$ and 2.

2.2. Governing equations

The motion of an incompressible fluid with constant viscosity, μ, and density, ρ, can be described using the unsteady incompressible Navier-Stokes equations,

$$\frac{\partial \mathbf{U}}{\partial t} + \mathbf{U} \cdot \nabla \mathbf{U} + \nabla P = \frac{1}{Re} \nabla^2 \mathbf{U}; \qquad \nabla \cdot \mathbf{U} = 0, \tag{1}$$

where $\mathbf{U}$ is the fluid velocity, P the reduced pressure and $Re = \overline{U} D/\nu$ is the Reynolds number, with $\nu = \mu/\rho$ denoting the kinematic viscosity. Here, all terms are non-dimensionalized using a typical length scale, D, and velocity, $\overline{U}$, which are chosen as the hydraulic diameter and the bulk velocity of the mixing channel, respectively. It is also worth noting that in our case, since $\kappa_o = 2\kappa_i$, the bulk velocity in the mixing channel is the same as that of the inlet channels.

No-slip boundary conditions are imposed at the mixer walls, while, at the inlet, a unidirectional fully developed velocity profile is assumed. The latter can be derived by solving the steady-state Navier-Stokes equation with no-slip boundary conditions at the walls and subjected to a constant axial pressure gradient G. In this way, the following velocity profile is obtained (Chatwin and Sullivan, 1982; Happel and Brenner, 1965)

$$U\left(y,z\right)=-\frac{G}{2\mu}y\left(Y-y\right)-\frac{4GY^{2}}{\mu\pi^{3}}\sum_{k\,odd}C_{k}(z)\sin\left(k\pi\frac{y}{Y}\right), \tag{2}$$

where,

$$C_{k}(z)=\frac{1}{k^{3}}\left[\cosh\left(k\pi\frac{z}{Y}\right)-\tanh\left(\frac{k\pi}{2\eta}\right)\sinh\left(k\pi\frac{z}{Y}\right)\right]. \tag{3}$$

Here, x is the longitudinal axis, while y and z are the transversal axes, with Y and Z denoting the sizes of the conduit and $\eta=Y/Z$ the conduit aspect ratio (in our case, $Y=W_i$, $Z=H$, and $\eta=\kappa_i$.) From this expression, the pressure gradient G can be derived as a function of the mean velocity $\overline{U}$, finding:

$$G=-\frac{12\mu}{Y^{2}}\overline{U}\left[1-\frac{192}{\pi^{5}}\sum_{k\,odd}\frac{1}{k^{5}}\tanh\left(\frac{k\pi}{2\eta}\right)\right]^{-1}. \tag{4}$$

2.3. Numerical model

The numerical model was developed using the Nek5000 code, a massively parallel open source solver for the incompressible Navier-Stokes equation, based on a high-order spectral element method (Fisher, 1997). The basis functions inside each element consist of Legendre polynomials of N-th order for velocity, and $(N-2)$-th order for pressure, with typically $N\geq 6$.

These polynomials are the Lagrangian interpolants based on tensor-product arrays of the Gauss-Lobatto-Legendre (GLL) quadrature points in each hexahedral element. It can be shown that the method has both a spectral convergence in N (i.e., the so-called p-refinement), and the convergence of a high order finite element method with respect to the number of elements (i.e., the so-called h-refinement). Time discretization uses a third order explicit backward-differentiation of the convective terms, and an implicit scheme for the viscous terms. A validation of the numerical tools built in the framework of NEK5000 for stability and sensitivity analysis can be found in Fani et al. (2013). The results shown here have been obtained using a structured multi-block grid. Along the width of all the channels, a uniform element size is chosen, while along their axis the size varies. The polynomial order for the velocity is equal to 7. Globally, the used grids ranged from 12250 elements for $\kappa_i = 1$ to 22800 elements for $\kappa_i = 2$, associated to 4.0 10^6 and 7.5 10^6 degrees of freedom for the velocity, respectively. As concerns the time discretization, a constant time step equal to 7.0 10^{-4} is adopted, corresponding to a CFL number equal to 0.3.

Typically, a single DNS configuration required about 80,000 CPU hours and was carried out using 2048 cores, thanks to a High Performance Computing platform.

3. Results

Simulations were carried out for all the considered configuartions by progressively increasing the Reynolds number. Table 2 reports the Reynolds numbers at which the transition between different regimes (i.e. steady sym-

Table 2: Effect of aspect ratio on the onset of different regimes

κ_i	Re (St Asym)	Re (Unst Asym)	Re (Unst Sym)	Re (Chaotic)
0.75	140	220	400	560
1	138	240	335	515
2	-	-	420-450	550

metric, steady asymmetric, unsteady asymmetric, unsteady symmetric and chaotic) was observed for the three aspect ratios investigated.

3.1. Steady symmetric (vortex) regime

At low Reynolds numbers, the flow in the $\kappa_i = 1$ T-mixer, is typically characterized by two pairs of counter-rotating vortical structures, originating in the recirculation region near the walls of the mixer, at the confluence of the two inlet streams: this regime has been characterised both experimentally and numerically (see Engler et al., 2004; Hoffmann et al., 2006; Bothe et al., 2006; Kockmann and Roberge, 2011) and is denoted as vortex regime. Figure 2 shows the vortical structures as identified through the λ_2 criterion (Jeong and Hussain, 1995) at $Re = 130$; λ_2 is the second largest eigenvalue of the tensor $(\mathbf{S}^2 + \mathbf{\Omega}^2)$, where $\mathbf{S}$ and $\mathbf{\Omega}$ are the symmetric and antisymmetric part of the velocity gradient tensor $\nabla\mathbf{U}$, i.e. the strain-rate and vorticity tensors. The presence of a vortex core is associated with a negative value of λ_2 (Jeong and Hussain, 1995). The λ_2 criterion measures the excess of rotation over strain rate on a specific plane. For flow at high Reynolds number this vortex-detection criterion coincides with the one based on the minimum of pressure, while it gives a better identification of vortex cores at low Reynolds numbers.

The y-direction vorticity and the on-plane velocity vectors are also reported for $y = -0.75$ and $y = -1.25$, clearly indicating a typical double mirror symmetry of the flow field. For that reason, in the following, the vortex flow will also be denoted as *steady symmetric regime*.

The morphology of the steady symmetric regime for the $\kappa_i = 0.75$ T-mixer is similar and described in details in Fani et al. (2013). Moreover, we see that for both $\kappa_i = 0.75$ and $\kappa_i = 1$ configurations the steady symmetric regime remains stable up to similar critical Reynolds numbers, i.e., $Re = 140$ and $Re = 138$, respectively (see Table 2), when a transition to the engulfment regime is observed. The above critical Re values are in very good agreement with the numerical simulations of Poole et al. (2013), who indicated $Re = 138$ for $\kappa_i = 1$, as well as $Re = 154$ and $Re = 137$ for $\kappa_i = 0.7$ and $\kappa_i = 0.8$, respectively.

When $\kappa_i = 2$, instead, the vortex regime remains stable up to very large Reynolds number, i.e. $Re \approx 435$, indicating that this case is fundamentally different than the previous ones. This is confirmed by the vortical structures at $Re = 420$, identified through the λ_2 criterion, that are shown in Figure 3. Indeed, the flow for $\kappa_i = 2$ exhibits always a double mirror symmetry, but with four pairs of main counter-rotating vortices: the two pairs located closer to the mixer axis are stronger and they belong to the 3D vortical structures, which are present also for the two other considered T-mixer geometrie and originate from the separation regions at the confluence of the incoming flow streams at the top of the channel. The additional legs, which are weaker and more far from the axis, are fed by the flow separations occurring at the lower corners of the inlet channels. These additional separations are present

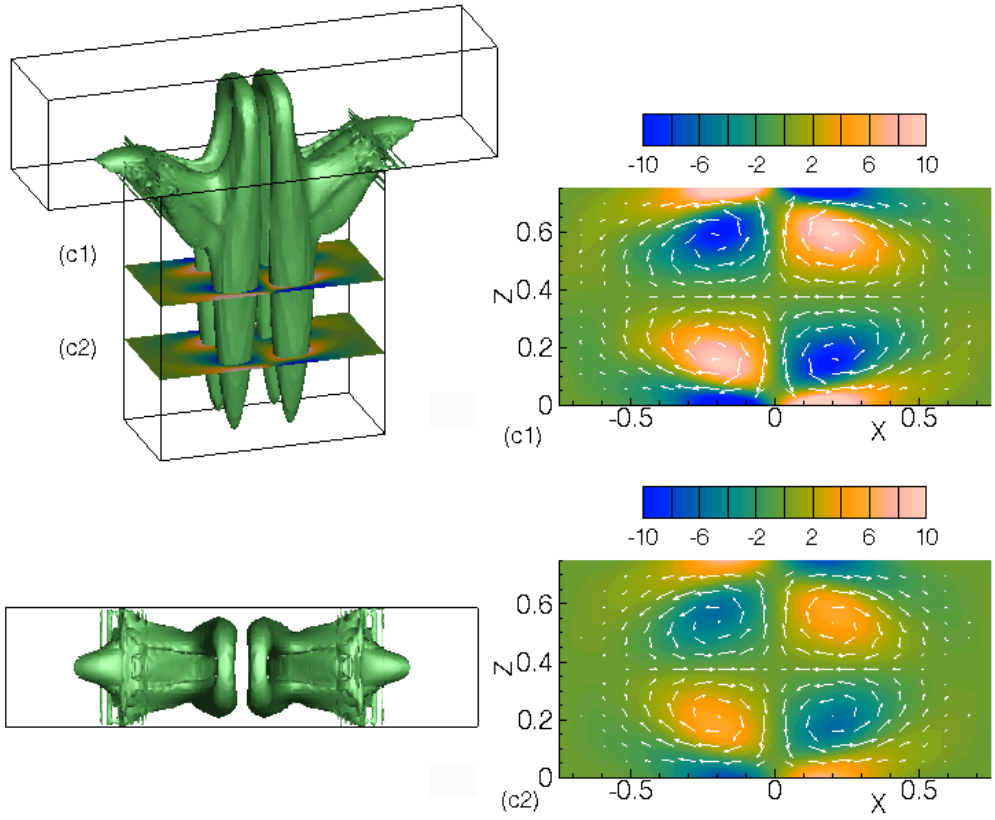

Figure 2: Identified vortices in the micro-mixer, contours of vorticity normal to the cutting plane and in-plane velocity vectors at sections (c1) $y = -0.75$ and (c2) $y = -1.25$ for the vortex regime. $Re = 130$, $\kappa_i = 1$.

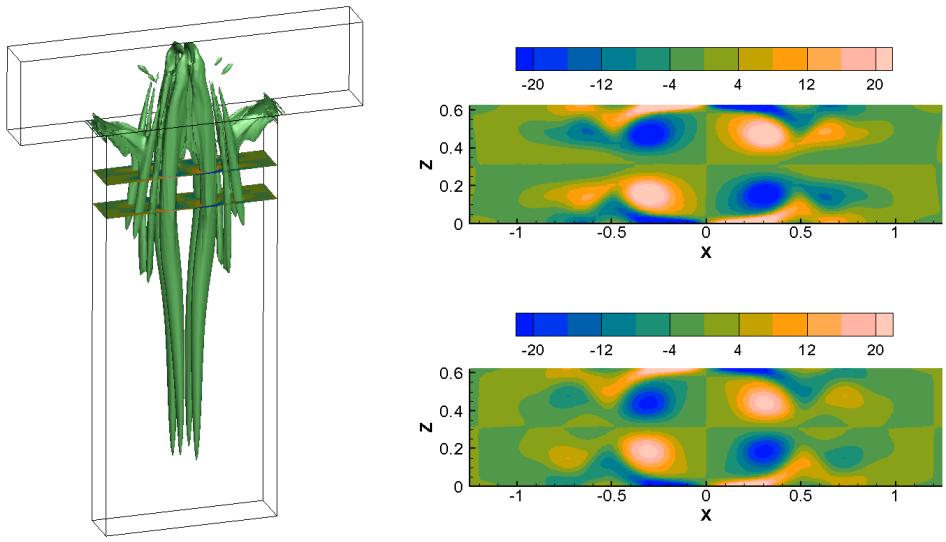

Figure 3: Identified vortices in the micro-mixer, contours of vorticity normal to the cutting plane at sections $y = -0.75$ and $y = -1.25$ for the vortex regime. $Re = 420$, $\kappa_i = 2$.

also for the two other considered T-mixer geometries (see Fig. 2), but for $\kappa_i = 0.75$ and 1, their vorticity merges with that of the stronger four legs of the main 3D structures. Conversely, for $\kappa_i = 2$, due to the more elongated section shape, the additional legs survive inside the mixing channel, as can be seen, for instance, from the vorticity field at two cross-sections of the mixing channel in Figure 3.

3.2. Steady asymmetric (engulfment) regime

For $\kappa_i = 0.75$ and $\kappa_i = 1$, as we increase Re up to $Re = 140$ and $Re = 138$, respectively, we observe a symmetry breaking, with a transition from steady symmetric (vortex) to engulfment regime, that is from mirror to point symmetry of the flow, i.e. the flow structures in the engulfment regime where the latter are invariant under point reflection through the center of

the outflow channel cross section. In the nomenclature used in Galletti et al. (2012) this is a transition from a C-shaped to an S-shaped morphology while here, in the following, the engulfment flow will also be denoted as *steady asymmetric regime*. The flow features observed in this regime for $k_i = 1$ are practically the same as those found for $k_i = 0.75$ and analyzed in details in Fani et al. (2013). Vortices identified through the λ_2 criterion for the steady asymmetric regime at $Re = 230$ are shown, for instance, in Figure 4 from two different views for $\kappa_i = 1$.

It is evident that the flow is characterized, as in the vortical regime, by two main 3D vortical structures, which are counter-rotating and made by a top part and by two legs entering the mixing channel. As shown in Fani et al. (2013), the top parts are inside the separation bubble which forms at the confluence between the two incoming streams. In the engulfment regime, the separation bubble, and hence the top parts of the 3D vortical structures, are tilted respect to the y-z plane (see, e.g., Fig. 4a). As a consequence, the legs entering the mixing channel are no more equal in terms of intensity, shape and position. This can be seen, for instance, in Figure 5, where the normal vorticity and the on-plane velocity are reported at different cross sections, $y = -0.75, -1.25, -2, -3$ when, again, $Re = 230$ and for $\kappa_i = 1$. We see that, at the confluence of the inlet streams, the flow field is characterized by two pairs of more intense co-rotating vortical structures and by two additional, weaker vortical structures (5a), that progressively merge with the main vortices as they move along the mixing channel (Figures 5c-d) until, further down, only a pair of co-rotating vortices remain, almost aligned with the axis of the mixing channel. Such co-rotating vortices, and

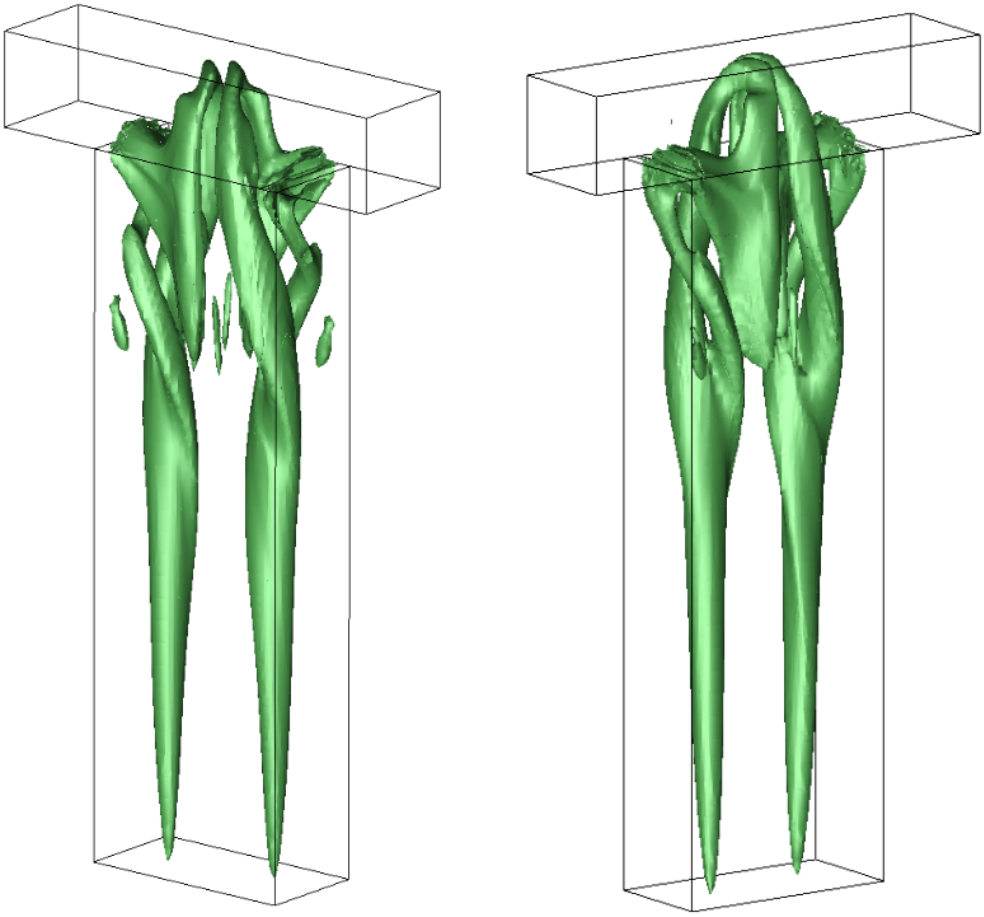

Figure 4: Two different views of vortices identified through the λ_2 criterion in the micro-mixer for the steady asymmetric (engulfment) regime. $Re = 230$, $\kappa_i = 1$.

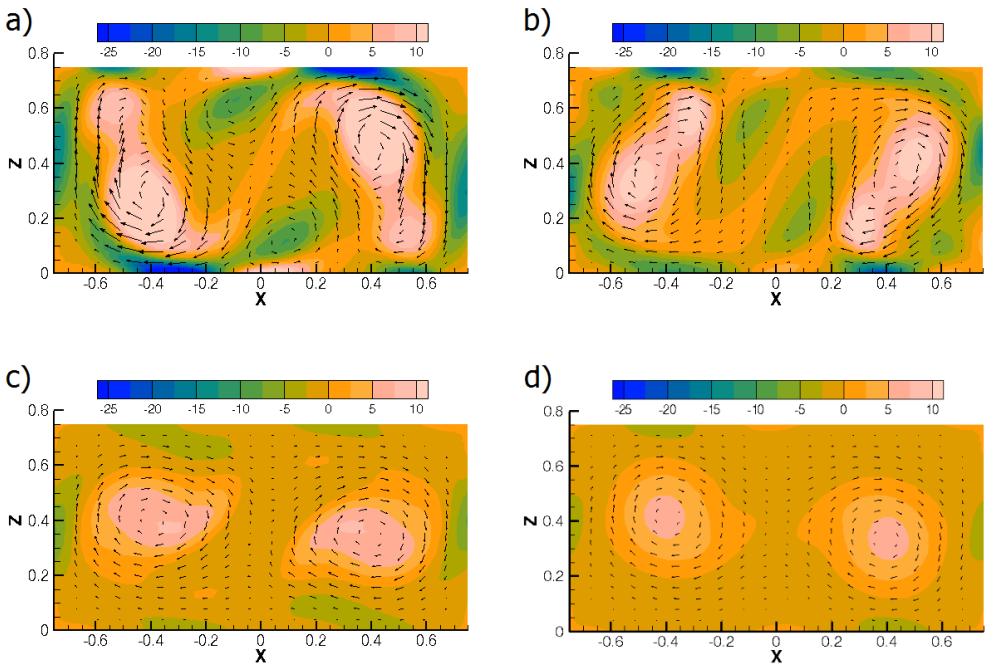

Figure 5: Vorticity normal to the cutting plane and in-plane velocity vectors for the steady asymmetric (engulfment) regime at mixing channel sections: (a) $y = -0.75$, (b) $y = -1.25$, (c) $y = -2$, (d) $y = -3$. $Re = 230$, $\kappa_i = 1$.

the resulting loss of mirror symmetry, are responsible for a huge increase in the degree of mixing between the two incoming streams when we pass from vortex to engulfment regime, as observed in many previous works (e.g., see Engler et al. 2004; Bothe et al., 2006; Hoffmann et al., 2006; Galletti et al., 2012). For further details about the origins and stability of the steady asymmetric regime, please refer to Fani et al. (2013), and references therein.

Conversely, when $\kappa_i = 2$, the channel is so large that symmetry breaking is inhibited: as a consequence, no steady asymmetric regime is observed for such configuration. The absence of a steady asymmetric (engulfment) regime was also observed by Poole et al. (2013) but for T-mixers configurations that are much different than the present one, e.g. for $\kappa_o = 0.375$ and $\kappa_i = 1$, or $\kappa_o = 0.65$ and $\kappa_i = 0.65$.

3.3. Unsteady asymmetric regime

For the T-mixer configurations with $k_i = 0.75$ and 1, when the Reynolds number is further increased beyond a second critical value, transition to a periodic regime denoted as *unsteady asymmetric regime* occurs. Once again the transition threshold values of the Reynolds number are similar for the two configuration, namely 220 for $k_i = 0.75$ and 240 for $k_i = 1$ (see Table 2). Also for this regime, the flow morphology and dynamics for $k_i = 1$ are very similar to those of the configuration having $k_i = 0.75$, reported and analyzed in detail in Fani et al. (2014). Six snapshots of the periodic flow regime for the $\kappa_i = 1$ T-mixer at $Re = 280$ are reported in Figure 6; these snapshots span a flow cycle. Figure 6a, in which the flow morphology is very similar to that of the engulfment regime has arbitrarily been chosen as the beginning of the cycle. The top parts of the two main vortical structures tend

to approach each other, and, as they approach their tilting angle increases (Figure 6b and Figure 6c). Since they contain vorticity of opposite sign, they quickly annihilate as well as the tilted recirculation bubble, from which they originated (Figs 6e). The strong legs of the two structures also merge and form a blob of vorticity which is rapidly convected through the outlet channel; a trace of the passage of this blob can be seen, for instance, in Figure 6e (top plane section). The passage of the blob also causes the twisting of the legs of the vortices (Figure 6b, 6c and 6d). In the meanwhile, the top parts of two new vortical structures form in two new separation regions near the top corners of the mixer (Figure 6d and 6e), which progressively travel towards the center of the mixer and create two strong legs entering the outlet channel, which replace the original ones. The cycle then starts again.

As mentioned previously, no evidence of this regime was found for the T-mixer with $\kappa_i = 2$.

3.4. Unsteady symmetric regime

For $\kappa_i = 0.75$, transition from unsteady asymmetric to the so-called *unsteady symmetric regime* was observed to occur at $Re = 400$. The snapshots taken for the unsteady symmetric regime at $Re = 480$ are reported in Figure 7. It can be noticed that the flow oscillates between symmetric (e.g. Figure 7c) and asymmetric states (e.g. Figure 7e). The former are characterised by four legs in the mixing channels as in the steady vortical regime, whereas the latter presents two main legs as in the steady engulfment. Therefore, for this aspect ratio the flow preserves some degree of asymmetry also in this new regime. A more detailed description of the unsteady symmetric regime for $\kappa_i = 0.75$ can be found in Fani et al. (2014).

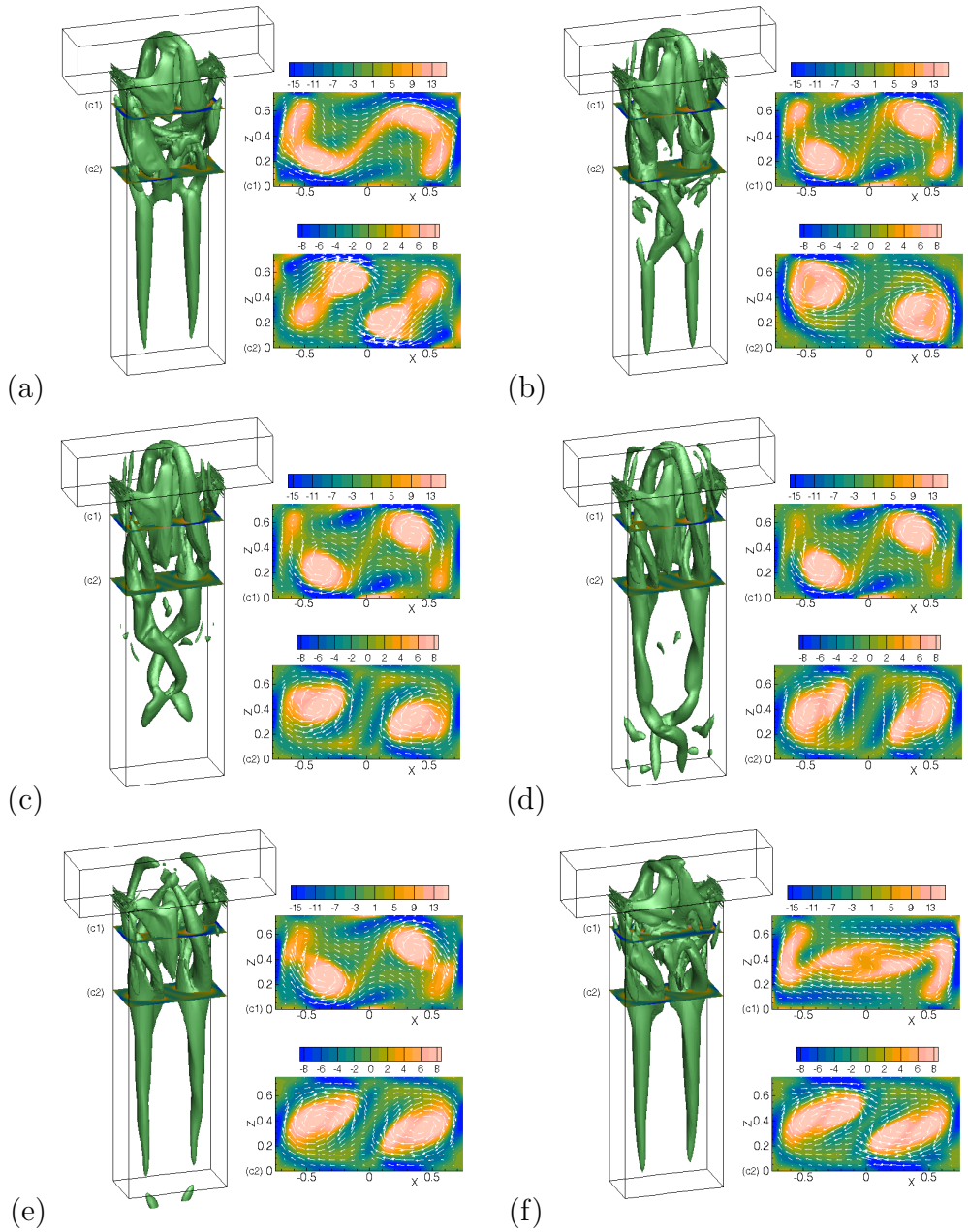

Figure 6: Vortices identified through the λ_2 criterion in the micro-mixer, contours of vorticity normal to the cutting plane and in-plane velocity vectors at sections $y = -0.5$ and $y = -1.5$ for the unsteady asymmetric regime. Snapshots at times $t/T \approx$ (a) 0, (b) 0.15, (c) 0.28, (d) 0.56, (e) 0.77, (f) 0.90, where T is the flow period. $Re = 280$, $\kappa_i = 1$.

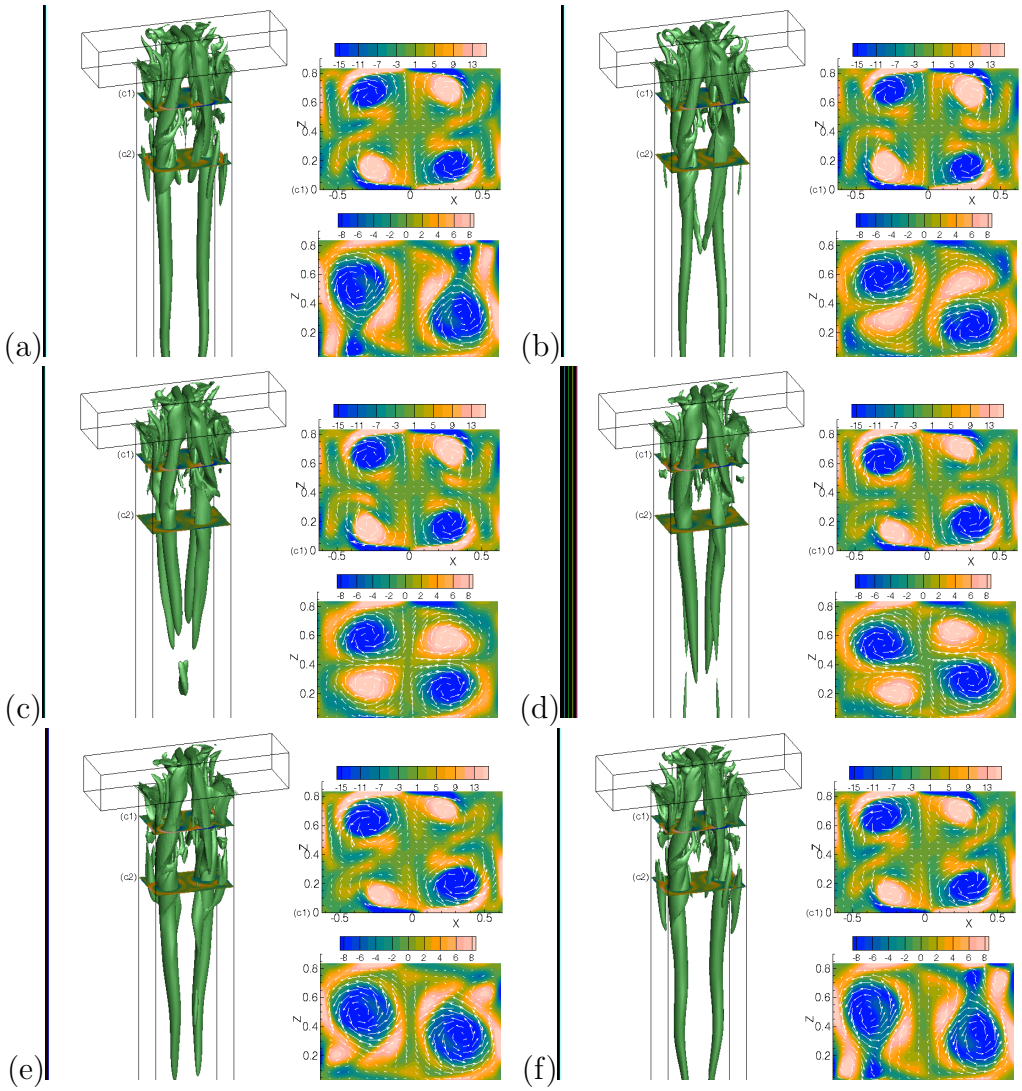

Figure 7: Vortices identified through the λ_2 criterion in the micro-mixer, contours of vorticity normal to the cutting plane and in-plane velocity vectors at sections $y = -0.5$ and $y = -1.5$ for the unsteady symmetric regime. Snapshots at times $t/T \approx$ (a) 0, (b) 0.18, (c) 0.36, (d) 0.55, (e) 0.73, (f) 0.91, where T is the flow period. $Re = 480$, $\kappa_i = 0.75$.

For $\kappa_i = 1$, a new periodic unsteady regime is also observed as the Reynolds number is further increased above $Re = 335$. However, at difference with the configuration having $\kappa_i = 0.75$, the flow always maintains a double mirror symmetry and it is characterized by two pairs of counter-rotating vortical structures, originating at the confluence of the two inlet streams, with four legs, approximately of the same intensity, well visible in the mixing channel figure as in the steady vortex regime (see e.g.Fig. 8 which refers to $Re = 450$) . The flow unsteadiness is mainly given by a periodic small oscillation of the top parts of the 3D vortical structures roughly in the x direction, as can be seen in Figure 9; this leads also to small changes in the position and shape of the four legs (compare e.g. Fig. 8(a) and 8(b)). Thus, for $\kappa_i = 1$ the degree of mixing in the unsteady symmetric regime is expected to be dramatically reduced compared to that of the engulfment and of the unsteady asymmetric regimes. This is in agreement with the experimental work of Thomas et al. (2010) and Thomas and Ameel (2010), who concluded that this regime is less effective for mixing than the unsteady asymmetric one.

The unsteady symmetric regime was also observed for the configuration with $\kappa_i = 2$. As mentioned previously, the larger aspect ratio seems to suppress both steady and unsteady asymmetric regimes, so that the T-mixer experiences a sudden transition from the steady symmetric (vortex) to the unsteady symmetric regime. The transition occurs between approximately $Re = 420$ and $Re = 450$. Actually, a precise Reynolds number could not be identified as significant hysteresis was observed. In fact, the numerical results that are obtained when Re is gradually increased, starting from a

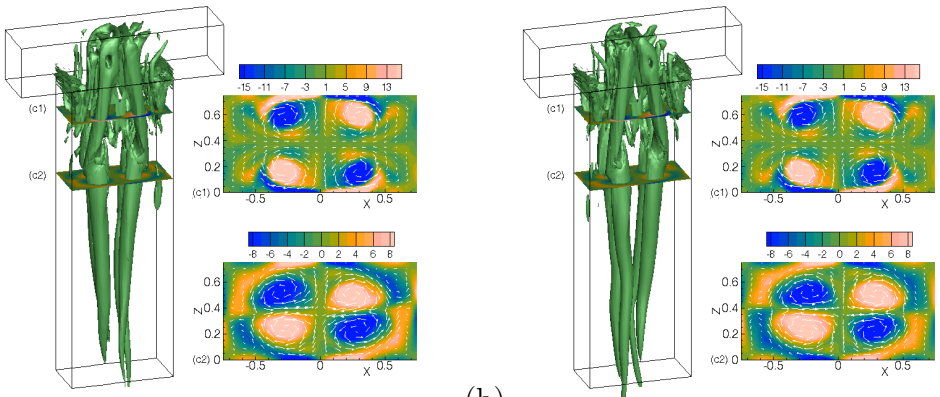

Figure 8: Vortices identified through the λ_2 criterion in the micro-mixer, contours of vorticity normal to the cutting plane and in-plane velocity vectors at sections $y = -0.5$ and $y = -1.5$ for the unsteady symmetric regime. Snapshots at times $t/T \approx$ (a) 0 and (b) 0.43, where T is the flow period. $Re = 450$, $\kappa_i = 1$.

steady symmetric morphology, appear to be different from those obtained when Re is gradually decreased. This type of hysteresis was also observed by Poole et al. (2013) for the determination of the critical Reynolds number for the engulfment regime, in case of T-mixers with low aspect ratios. The snapshots corresponding to the unsteady symmetric regime (at $Re = 500$) for a $\kappa_i = 2$ T-mixer are reported in Figure 10. It can be noticed that, as for $\kappa_i = 1$, the double mirror flow symmetry is preserved, but in this case there is the constant presence of eight main legs, as already observed for this aspect ratio in the steady vortical regime. The flow unsteadiness, also in this case, is given by small oscillations of the 3D vortical structures.

3.5. Chaotic regime

With a further increase of the Reynolds number, the periodicity of the flow disappears and the regime becomes chaotic. For $\kappa_i = 1$, the onset of

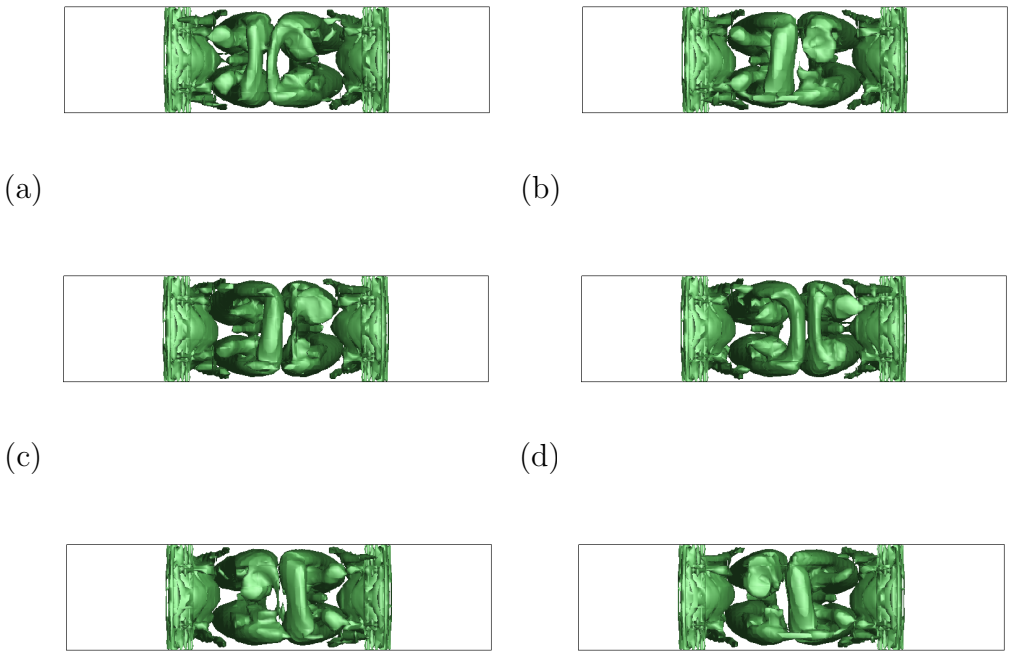

Figure 9: Vortices identified through the λ_2 criterion in the micro-mixer, contours of vorticity normal to the cutting plane and in-plane velocity vectors at sections $y = -0.5$ and $y = -1.5$ for the unsteady symmetric regime. Snapshots at times $t/T \approx$ (a) 0, (b) 0.14, (c) 0.43, (d) 0.57, (e) 0.71, (f) 0.86, where T is the flow period. $Re = 450$, $\kappa_i = 1$.

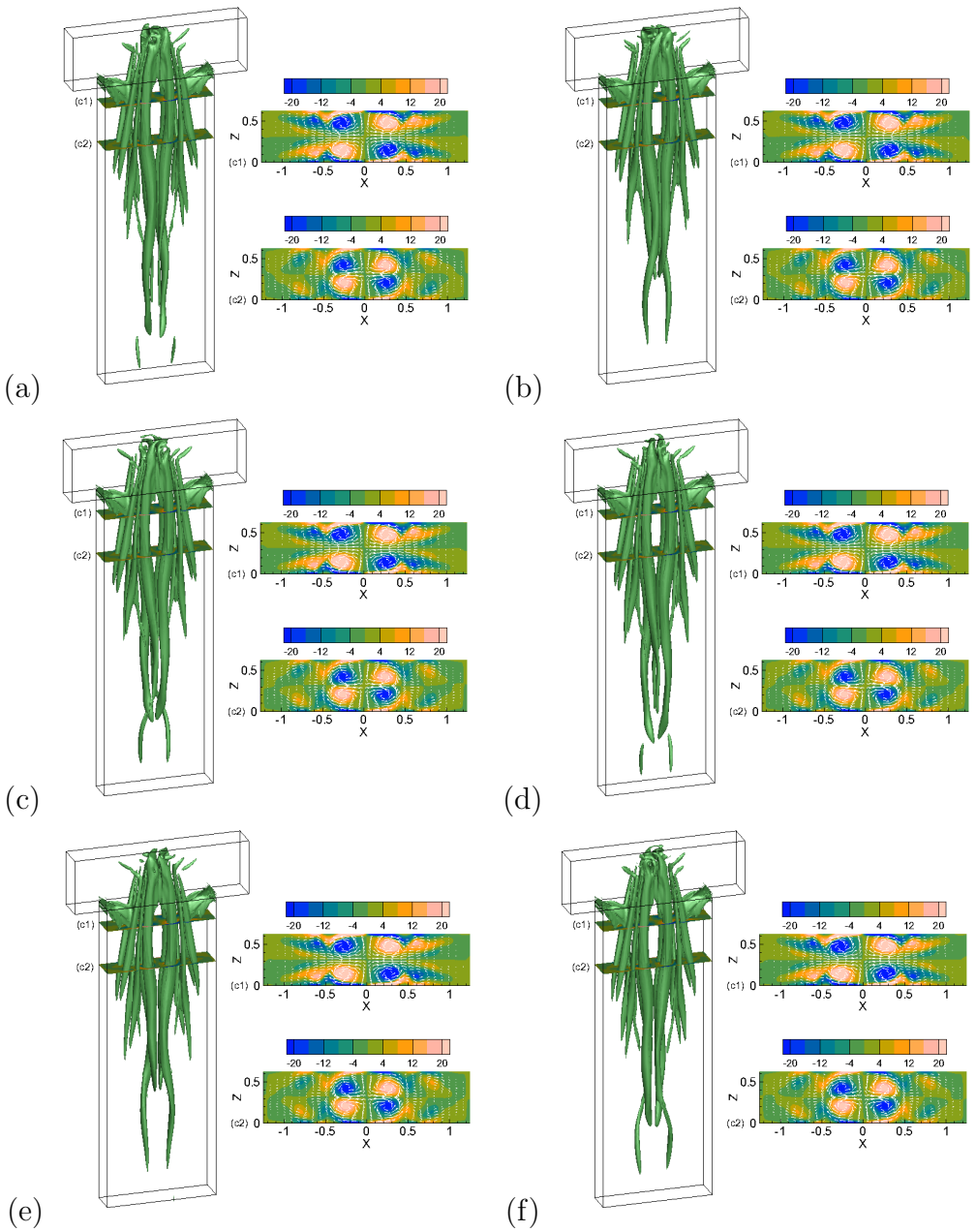

Figure 10: Vortices identified through the λ_2 criterion in the micro-mixer, contours of vorticity normal to the cutting plane and in-plane velocity vectors at sections $y = -0.5$ and $y = -1.5$ for the unsteady symmetric regime. Snapshots at times $t/T \approx$ (a) 0, (b) 0.18, (c) 0.35, (d) 0.53, (e) 0.71, (f) 0.88, where T is the flow period. $Re = 500$, $\kappa_i = 2$.

this *chaotic regime* occurs at a critical Reynolds number, $Re = 510 - 515$, although this value may be dependent on the channel length L_o/D, as longer mixing channels tend to stabilize the flow field by decreasing possible flow perturbation due to the outflow boundary conditions. In fact, the transition between periodic and random regime occurs at $Re = 500$ when $L_o/D = 22.5$ (in agreement with Dreher et al., 2009), whereas for $L_o/D \geq 33.75$ the critical Reynolds number increases to $Re = 515$, while we observed that the flow is still periodic at $Re = 510$. As reported in Table 2 the transition to the chaotic regime occurs at similar Reynolds numbers for all the investigated aspect ratios, being at $Re = 560$ and $Re = 550$ for $\kappa_i = 0.75$ and $\kappa_i = 2$, respectively.

3.6. Frequency analysis of unsteady regimes

In Figure 11 the Strouhal number, based on mixing channel hydraulic diameter and mean velocity, i.e. $St = fD/\overline{U}$, is represented as a function of Re for the different aspect ratios that have been investigated. The Strouhal number has been computed from the velocity signals recorded on the centerline of the mixing channel at different locations on the y axis. The uncertainty on the computed Strouhal numbers has also been estimated; the largest uncertainties occur when approaching the chaotic regime and they are the following: ± 0.008 for $\kappa_i = 2$ at $Re = 500$, ± 0.007 for $\kappa_i = 1$ at $Re = 510$ and ± 0.0095 for $\kappa_i = 0.75$ at $Re = 500$. For all the considered aspect ratios, at lower Reynolds numbers, the observed unsteady regimes are almost perfectly periodic and, hence, the uncertainty on St is practically negligible. It can be noticed that for $\kappa_i = 1$ the St number increases from $St = 0.24$ at the onset of the unsteady regime ($Re = 240$) to $St = 0.28$ when

$Re = 360$, subsequently it slightly decreases to $St = 0.26$ when $Re = 450$ and then increases again to $St = 0.30$ when $Re = 500$. These values are in good agreement with the results by Dreher et al. (2009) and with those by Minakov et al. (2012), that were obtained for the same geometrical configuration and are reported in Fig. 11 as well. For $\kappa_i = 0.75$, up to $Re \approx 400$, the Strouhal number monotonically increases with Reynolds and its values are similar to those obtained for $\kappa_i = 1$. As Re increases from 400 to 440, though, the frequency drops from 0.31 to 0.11, and then, for larger Re, it remains at similar values, which are significantly lower than those found for $\kappa_i = 1$ at the same Reynolds numbers. Since this Re range corresponds to the unsteady symmetric regime, the differences in the Strouhal number between the two configurations might be explained by the different behaviors observed in this regime as described in Sec. 3.4; we recall, in particular, that for $\kappa_i = 0.75$ the flow switches within a time period from a symmetric to an asymmetric vorticity configuration. Finally, for $\kappa_i = 2$ only the unsteady symmetric regime exists for $Re > 450$ with Strouhal number values which are only slightly lower than the corresponding ones for $\kappa_i = 1$. This is again consistent with the similar flow dynamics observed in this regime for $\kappa_i = 1$ and $\kappa_i = 2$.

4. Conclusions

The different flow regimes occurring in T-mixers are investigated using Direct Numerical Simulations, for three values of the aspect ratios of the inlet channels, i.e. their width-to-height ratio, $\kappa_i = 0.75$, 1 and 2. The problem was scaled in terms of the hydraulic diameter, D, and the bulk fluid velocity,

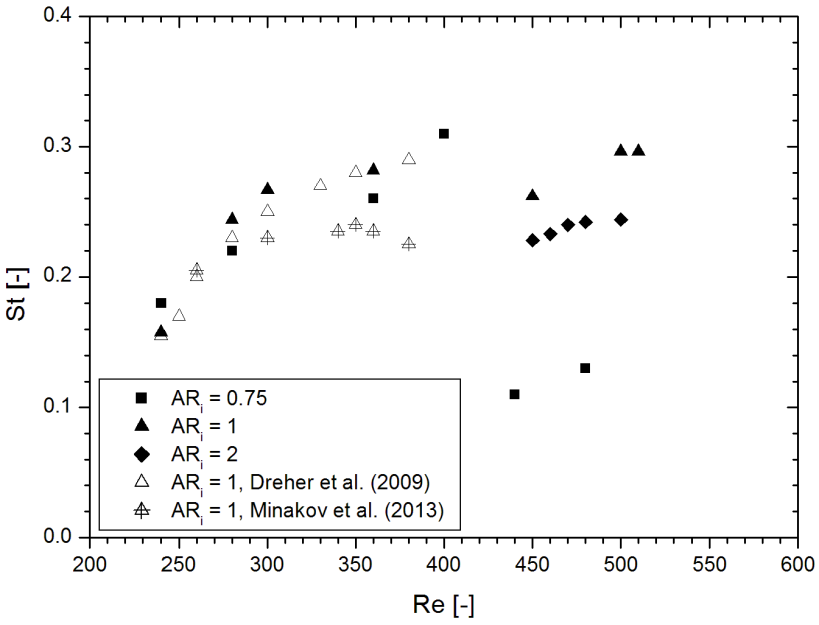

Figure 11: Strouhal number as a function of the Reynolds number for different aspect ratios $\kappa_i = 1$.

the latter being the same in the inlet and in the mixing channels.

At low Reynolds numbers, a steady regime presenting a double mirror symmetry, known as vortex regime, is observed for all the considered configurations. However, for $\kappa_i = 2$ the topology of the vorticity field is different with four pairs of main counter rotating vortices in the mixing channel instead of the two pairs observed for the other geometries.

The $\kappa_i = 0.75$ and $\kappa_i = 1$ T-mixers behave similarly for increasing Reynolds number, showing first the occurrence of the steady asymmetric regime, also denoted as engulfment flow, which is invariant under point reflection through the center of a cross section. The critical value of Re for the onset of the engulfment regime is also practically the same for the two configurations, i.e. $Re = 138 - 140$. By further increasing the Reynolds number, above $Re = 220 - 240$, the vorticity configuration which characterizes the engulfment regime becomes unstable and the flow field turns to be time periodic, although still retaining its point central symmetry. In this, so called, unsteady asymmetric regime, the characteristic Strouhal number (or the non dimensional time frequency) is found to increase with Reynolds in the range $St \approx 0.16 - 0.3$, in agreement with the results of previous studies. Then, at $Re = 335 - 350$, again for both $\kappa_i = 0.75$ and 1, the flow field switches to another time-periodic regime, called unsteady symmetric regime. Some differences between the two configurations, though, were observed in the unsteady symmetric regime: for $\kappa_i = 1$ this regime was always characterized by a double mirror symmetry (four-vortex topology), whereas when $\kappa_i = 0.75$ the flow alternates between the symmetric and asymmetric states. Moreover for $\kappa_i = 1$, the characteristic frequency is about the same as that

of the asymmetric regime, i.e., with $St \approx 0.3$. Conversely, the $\kappa_i = 0.75$ T-mixer shows a significant reduction of the Strouhal number, down to about $St = 0.1 - 0.15$ at the transition from unsteady asymmetric to unsteady symmetric regime. These low St values seem to be related to the oscillations between the symmetric and asymmetric states.

The flow behavior for the largest aspect ratio was found to be significantly different than that corresponding to $\kappa_i \leq 1$, previously described, as the flow field appears to favor configurations with mirror symmetry. Indeed, for $\kappa_i = 2$, the flow regime remains steady and symmetric up to $Re \approx 430$, when it becomes unsteady, but still maintains its double mirror symmetry. In other words, no steady asymmetric (engulfment) and unsteady asymmetric regimes are observed, but the flow passes directly from the steady vortical to the unsteady symmetric regime. In this latter regime, the behavior is similar to that observed for $\kappa_i = 1$, i.e. the flow is always characterized by a double mirror symmetry, but in this case with a four vortex-pair topology, i.e. the same already observed for the steady vortical regime in this configuration. The characteristic Strouhal number values are also similar to those obtained for $\kappa_i = 1$.

Finally, in all cases, at larger Re, the flow regime ceases to be periodic and becomes chaotic. This last transition occurs for $Re = 515 - 560$.

As a final remark, the present results suggest that, for low Reynolds numbers, before transition to the chaotic regime, large aspect ratios can be detrimental for mixing, because of the tendency of the flow to keep a mirror symmetry. Moreover, the remarkable differences in the flow behavior observed for $\kappa_i = 2$ confirm the difficulty in finding correlations valid for a

large range of geometries.

Acknowledgments

The authors wish to thank CINECA computing center (Bologna, Italy) for allowance of computational resources on FERMI supercomputer under the ISCRA programme.

Bothe D, Stemich C, Warnecke HJ. Fluid mixing in a T-shaped micro-mixer. Chem Eng Sci, 2006; 61: 2950-2958.

Bothe D, Stemich C, Warnecke HJ. Computation of scales and quality of mixing in a T-shaped microreactor. Comput Chem Eng 2008; 32: 108-114.

Chatwin PC, Sullivan PJ. The effect of aspect ratio on the longitudinal diffusivity in rectangular channels. J Fluid Mech 1982; 120: 347-358.

Cherlo SKR, Pushpavanam S. Effect of depth on onset of engulfment in rectangular micro-channels. Chem Eng Sci 2010; 65: 6486-6490.

Dreher S, Kockmann N, Woias P. Characterization of laminar transient flow regimes and mixing in T-shaped micromixers. Heat Trans Eng 2009; 30: 91-100.

Engler M, Kockmann N, Kiefer T, Woias P. Numerical and experimental investigations on liquid mixing in static micromixers. Chem Eng J 2004; 101: 315-322.

Fani A, Camarri S, Salvetti MV. Stability analysis and control of the flow in a symmetric channel with a sudden expansion. Phys Fluids 2012; 24: 084102.

Fani A, Camarri S, Salvetti MV. Unsteady asymmetric engulfment regime in a T-mixer. Phys Fluids 2014; 26: 074101.

Fani A, Camarri S, Salvetti MV. Investigation of the steady engulfment regime in a three-dimensional T-mixer. Phys Fluids 2013; 25: 064102.

Fisher PF. An overlapping Schwarz method for spectral element solution of the incompressible Navier-Stokes equations. J Comput Phys 1997; 133: 84101.

Galletti C, Roudgar M, Brunazzi E, Mauri R. Effect of inlet conditions on the engulfment pattern in a T-shaped micro-mixer. Chem Eng J 2012; 185-186: 300-313.

Happel J, Brenner H. Low Reynolds Number Hydrodynamics. Englewood Cliffs, NJ: Prentice Hall; 1965. Eq. (2-5.24).

Hoffmann M, Schlüter M, Räbiger N. Experimental investigation of liquid-liquid mixing in T-shaped micro-mixers using μ-LIF and μ-PIV. Chem Eng Sci 2006; 61: 2968-2976.

Kockmann N, Roberge DM. Transitional Flow and Related Transport Phenomena in Curved Microchannels, Heat Transfer Eng 2011; 32: 595-608.

Kumar V, Paraschivoiu M, Nigam KDP. Single-phase fluid flow and mixing in microchannels. Chem Eng Sci 2011; 66: 1329-1373.

Jeong J, Hussain F. On the identification of a vortex. J. Fluid Mech. 1995; 285: 69-94.

Lindken R, Westerweel J, Wieneke B. Stereoscopic micro particle image velocimetry. Exp Fluids 2011; 32: 595-608.

Lindken R, Westerweel J, Wieneke B. Stereoscopic micro particle image velocimetry. Exp Fluids 2011; 32: 595-608

Minakov AV, Rudyak VYa, Gavrilov AA, Dekterev AA. Mixing in a T-shaped micromixer at moderate Reynolds numbers. Thermophys Aeromech 2012; 19: 385-395.

Minakov AV, Rudyak VYa, Dekterev AA, Gavrilov AA. Investigation of slip boundary conditions in the T-shaped microchannel. Int J Heat Fluid Fl 2013; 43: 161-169.

Ooms TA, Lindken R, Westerweel J. Digital holographic microscopy applied to measurement of a flow in a T-shaped micromixer. Exp Fluids 2009; 47(6): 941-955.

Poole RJ, Alfateh M, Gauntlett AP. Bifurcation in a T-channel junction: Effects of aspect ratio and shear-thinning. Chem Eng Sci 2013; 104: 839-848.

Soleymani A, Yousefi H, Turunen I. Dimensionless number for identification of flow patterns inside a T-micromixer. Chem Eng Sci 2008; 63: 5291-5297.

Thomas S, Ameel T, Guilkey J. Mixing kinematics of moderate Reynolds number flows in a T-channel. Phys. Fluids 2010; 22: 013601.

Thomas S, Ameel T. An experimental investigation of moderate Reynolds number flow in a T-Channel. Exp Fluids 2010; 49: 1231-1245.